# Controlled site coverage of strong metal-support interaction (SMSI) on Pd NP catalysts

| Journal: | *Catalysis Science & Technology* |
|---|---|
| Manuscript ID | CY-ART-09-2022-001707.R1 |
| Article Type: | Paper |
| Date Submitted by the Author: | 07-Nov-2022 |
| Complete List of Authors: | Breckner, Christian; Purdue University, Davidson School of Chemical Engineering<br>Zhu, Kuixin; Purdue University, Department of Chemistry<br>Wang, Mingrui; PSU-DUT Joint Center for Energy Research, State Key Laboratory of Fine Chemicals, School of Chemical Engineering, Dalian University of Technology, Dalian 116024, PR China<br>Zhang, Guanghui; Dalian University of Technology, State Key Laboratory of Fine Chemicals, PSU-DUT Joint Center for Energy Research, School of Chemical Engineering<br>Li, Christina; Purdue University, Department of Chemistry<br>Miller, Jeffrey; Purdue University, Chemical Engineering |
| | |

SCHOLARONE™
Manuscripts

# Controlled site coverage of strong metal-support interaction (SMSI) on Pd NP catalysts

Christian Breckner,[1] Kuixin Zhu,[2] Mingrui Wang,[3] Guanghui Zhang,[3] Christina W. Li,[2] and Jeffrey T. Miller[1*]

[1] Davidson School of Chemical Engineering, Purdue University, West Lafayette, IN 47907, United States. E-mail: mill1194@purdue.edu

[2] Department of Chemistry, Purdue University, West Lafayette, Indiana 47907, United States. E-mail: christinawli@purdue.edu

[3] State Key Laboratory of Fine Chemicals, Frontiers Science Center for Smart Materials Oriented Chemical Engineering, PSU-DUT Joint Center for Energy Research, School of Chemical Engineering, Dalian University of Technology, Dalian, Liaoning, 116024, China. E-mail: gzhang@dlut.edu.cn

[*]Corresponding Author: mill1194@purdue.edu

**Abstract**

Strong metal-support interaction catalysts have shown to improve desired product selectivity at the cost of fractional rates due to active site coverage. The goal of this study was to determine if the active site coverage of metallic nanoparticles could be controlled to lower levels than have been previously reported in SMSI catalysts with the aim of improving the rate while maintaining high selectivity. 2Pd-XTi/SiO$_2$ (2 wt% Pd, X wt% Ti) strong metal-support interaction (SMSI) catalysts with Ti loadings between 0-1.0 wt% were synthesized to control Pd nanoparticle coverage. Calcination at 450 °C and reduction at 550 °C were sufficient for forming ~2 nm sized Pd particles in all catalysts. Increasing the Ti loading from 0.1 to 1.0 wt% increased the surface coverage from 40 to 85% at a fixed reduction temperature of 550 °C. The IR spectra of the SMSI catalysts were similar with a high fraction of linear bonded CO which was much higher than that of Pd nanoparticles of similar size. The SMSI overlayer could be removed by oxidation at 350 °C and re-reduction at 200 °C. EXAFS of the oxidized catalysts indicate that nearly full oxidation of the metallic nanoparticle was required to remove the SMSI overlayer. Oxidation temperatures from 30 to 300 °C partially oxidized the Pd nanoparticles and subsequent re-reduction at 200 °C partially decreases the SMSI coverage. The fractional surface coverage was determined by measuring the rate of propylene hydrogenation with and without the SMSI overlayer. Increasing the reduction temperature from 200 to 550 °C increased the SMSI coverage from 0 to 85% depending on the Ti loading and temperature. The range of coverages varied between ~10% with 0.1 wt% Ti after re-reduction at 300 °C and ~85% with 1 wt% Ti after reduction at 550 °C.

## 1. Introduction

Since the original report of strong metal-support interaction (SMSI) by Tauster, et al. where a 2 wt% $Pd/TiO_2$ catalyst initially reduced at 175 °C experienced a significant drop in CO uptake when further reduced at 500 °C[1], there has been continued interest in utilizing this phenomenon for improving catalyst performance. SMSI has been shown to improve product selectivity, catalyst lifetime, and process performance in reactions such as propane dehydrogenation[2], olefin and acetylene hydrogenation[3-5], Fischer Tropsch synthesis[6], the water gas shift reaction[7], and in electrocatalysis[8]. Dulub and coworkers used electron microscopy on a $Pt/TiO_2$ catalyst to better understand why SMSI occurs. It was observed that the $TiO_2$ support, after surface species mobilization and partial reduction[9], covered metal nanoparticles resulting in less active sites available for catalysis[10]. Further work by Tauster, et al. found that this coverage could be reversed under high temperature oxidation[1]. Related work found that the same process can occur on $Pt/CeO_2$ catalysts as well indicating that this effect is not strictly limited to $TiO_2$ supports[11]. Further studies on transition metal oxide supports revealed that SMSI can occur on most reducible metal oxide supports such as $TiO_2$[9], $CeO_2$[11,12], $Fe_3O_4$[13,14], $La_2O_3$, $Nb_2O_5$[15], $MnO_2$[16], and even partially modified supports such as Tantalum-doped $TiO_2$[8]. SMSI has also been observed on non-reducible metal oxide supports such as ZnO[17,18] and non-metal supports such as hydroxyapatite[19,20] and Boron Nitride[21] through different migration and coverage processes. The metal nanoparticles that facilitate SMSI are as varied as the supports that induce them: Pd[1], Pt[10,11], Ag[22], Au[19], Ni, Fe[21], Rh[6,23], and Co[24], among others. Many early studies have concluded that the covered nanoparticles experience an electronic interaction with the encapsulating SMSI oxides[1,6,25-27]. Recent studies suggest that SMSI is primarily a physical interaction where the uncovered active sites do not experience an electronic interaction with the nearby SMSI oxide species[2,28-30]. It is likely that this misunderstanding of strong electronic interactions arose due to reactive metal-support interactions (RMSI), a process in which the encapsulating SMSI oxide becomes fully reduced to form an alloyed nanoparticle which experiences electronic interactions[31].

While studies on SMSI oxide supports were useful in understanding the encapsulation process, they have been shown to display low activity, particularly at reaction temperatures of 500 °C and above as the metal active sites become covered to near completion. Addition of low loadings of SMSI oxides to catalysts on inert supports, e.g. $Pt-Ti/SiO_2$, also display lower chemisorption and catalytic activity at these high reaction temperatures[2,4,15]. Previous studies have

typically used SMSI oxide loadings of greater than 1 wt%. While these have improved rates compared to nanoparticles on SMSI supports and retained the benefits of increased selectivity, improved catalyst lifetime, and reduced leaching rates in liquid systems[2,24], the rates remain relatively low compared to catalysts without SMSI oxides. Other methods, such as atomic layer deposition (ALD) of metal oxides onto supported metal nanoparticles, have the same effect seen in these SMSI systems[24,29,32]. For both SMSI and ALD catalysts the loss of nanoparticle surface coverage is typically greater than 70%. Lower surface coverage may give desirable modifications to catalytic performance but at higher rate. Currently, however, there are no methods to control the SMSI surface coverage levels below 70%.

In the present work, the goal was to determine if the active site coverage of metallic nanoparticles could be controlled to lower levels than have been previously reported in SMSI catalysts with the aim of improving the rate while maintaining high selectivity. Several methods are given to control the $TiO_{(2-x)}$ SMSI coverage of Pd nanoparticles from 10 to 80%. CO chemisorption, propylene hydrogenation rates, CO IR spectroscopy, STEM, and *in situ* X-ray absorption spectroscopy (XAS) are combined to show that the catalytic surface of ~2 nm sized Pd particles in 2Pd-XTi/SiO$_2$ SMSI catalysts (2 wt% Pd, X wt% Ti, SiO$_2$ support) can be partially covered by SMSI oxides in a controllable manner. A method to determine the fractional Pd surface coverage is also provided.

## 2. Materials and methods

### 2.1 Materials

Davisil 636 silica (99%), titanium(IV) bis(ammonium lactato)dihydroxide (50% solution), and tetraamminepalladium(II) nitrate (10% solution) were purchased from Sigma-Aldrich. All gases used for catalytic testing were purchased from Indiana Oxygen Company. 3% $C_3H_6$ and 5% $H_2$ were both balanced with $N_2$. The gases for XAS experiments were 3% $H_2$ balanced in He, pure He, and 10% $O_2$ balanced in He. All gases for XAS were purchased from AirGas, Illinois.

### 2.2 Catalyst preparation

The control, non-SMSI 2Pd/SiO$_2$ catalyst (0 wt% Ti, 2 wt% Pd) was synthesized using pH adjusted incipient wetness impregnation (IWI) on Davisil 636 silica (pore size = 60 Å, surface area = 480 m$^2$ g$^{-1}$). Ammonium hydroxide was added dropwise to a 10 wt% Pd(NH$_3$)$_4$(NO$_3$)$_2$ solution

diluted in deionized water until the pH was 11. This solution was added dropwise to Davisil 636 silica. The catalyst was dried overnight at 125 °C, split into thirds, and calcined at 450/600/700 °C for 3 hours each. The three catalysts were reduced in 5% $H_2/N_2$ (~100 mL min$^{-1}$) at 200 °C for 30 minutes and 250 °C for 30 minutes.

2Pd-XTi/SiO$_2$ (denoted as X wt% Ti containing catalyst throughout this paper, 2 wt% Pd) sequentially impregnated strong metal-support interaction (SMSI) were synthesized using sequential incipient wetness impregnation (IWI). Varied amounts of titanium(IV) bis(ammonium lactate) dihydroxide (50% solution) corresponding to 0.1/0.5/1.0 wt% Ti were diluted in deionized water and added dropwise to Davisil 636 silica. The XTi/SiO$_2$ catalyst precursors were dried overnight at 125 °C and calcined at 300 °C for 3 hours. A second solution containing 10 wt% tetraamminepalladium(II) nitrate solution diluted in deionized water was pH adjusted to 11 using ammonium hydroxide. This solution was added dropwise to the XTi/SiO$_2$ catalyst precursors to achieve a loading of 2 wt% Pd. The 2Pd-XTi/SiO$_2$ catalysts were dried overnight at 125 °C, split into thirds, and calcined at 450/600/700 °C for 3 hours each. The resulting 12 2Pd-XTi/SiO$_2$ catalysts were sequentially reduced in 5% $H_2/N_2$ (~100 mL min$^{-1}$) at 200 °C for 30 minutes and 250 °C for 30 minutes. SMSI was induced on the 2Pd-XTi/SiO$_2$ catalysts prior to analysis using a pre-treatment reduction temperature of 550 °C to initially stabilize particle sizes. The SMSI overlayer was removed using oxidation at 350 °C for 30 minutes. Analysis of the non-SMSI state was possible using a re-reduction temperature of 200 °C which did not induce SMSI coverage.

### 2.3  CO chemisorption

CO chemisorption was performed on a Micromeritics ASAP 2020 chemisorption instrument using a volumetric chemisorption analysis to determine relative particle sizes. A U-shaped quartz tube was filled with approximately 0.1 g of catalyst. The samples for the 2Pd/SiO$_2$ (0 wt% Ti) catalysts were reduced in 5% $H_2/He$ at temperatures ranging from 250-550 °C for 30 minutes prior to analysis at 30 °C. The 0.1-1.0 wt% Ti containing catalyst samples were reduced in 5% $H_2/He$ at 250 °C for 30 minutes. The 250 °C pre-treatment was used to determine if the SMSI catalysts had the same changes to relative particle size as the 2Pd/SiO$_2$ (0 wt% Ti) catalyst when increasing the calcination temperature. CO uptakes were estimated by taking the difference between the physisorption plus chemisorption and the physisorption only uptakes at different pressures. A linear regression of these points was used to estimate the uptake at zero pressure in

mmol CO/g metal. The sample loading and Pd wt% were used to convert to mol CO/mol metal. Pd nanoparticles can bind CO in a linear, bridging, or three-fold manner depending on the nanoparticle size. Larger Pd nanoparticles (> 4 nm) have predominately bridge bonding and three-fold bonding while small nanoparticles (< 4 nm) have a mixture of linear, bridge, and three-fold bonding. Higher reduction temperatures result in larger particle sizes and more face sites which cause the bonding factor to increase. This changing bonding factor makes it difficult to estimate particle sizes directly using only CO chemisorption.

### 2.4 Propylene hydrogenation catalytic performance tests

Propylene hydrogenation TORs at 30 °C were used to compare the performance of the catalysts. Rate measurements of the non-SMSI state were used in conjunction with Pd EXAFS dispersion estimates to calculate the TORs of all catalysts. The $2Pd/SiO_2$ (0 wt% Ti) catalyst was reduced at 250-550 °C then the rate was measured at 30 °C. For these reaction tests the 0.1-1.0 wt% Ti containing catalysts were reduced at 550 °C, oxidized at 350 °C, then re-reduced at 200-550 °C. The change in catalytic rate from the SMSI state (re-reduced between 300-550 °C) to the non-SMSI state (re-reduced at 200 °C) after the initial 550 °C reduction to stabilize particle size was used to estimate particle coverages. All catalytic tests were performed in a 12.7 mm ID quartz tube fixed bed reactor with a K-type thermocouple placed in the center of the bed to monitor the reaction temperature. A furnace connected to a temperature controller was used to manually adjust the bed temperature. Approximately 10 mg of catalyst was loaded into the reactor and was diluted to 1 g using $SiO_2$. The reactions were performed in 2.0% $H_2$ and 1.8% $C_3H_6$ balanced with $N_2$ at 30 °C. The products were analyzed using a Hewlett Packard 6890 GC with a flame ionization detector (FID). Peaks were integrated and compared to a bypass run of the mixed gases to determine conversion and catalytic rate. The catalytic rate was calculated using the conversion and initial propylene flow rate to obtain mol $C_3H_8 \cdot g_{cat}^{-1} \cdot s^{-1}$. The catalyst loading and Pd wt% were used to transform this to mol $C_3H_8 \cdot mol_{metal}^{-1} \cdot s^{-1}$. The TOR was calculated by dividing the catalytic rate in mol $C_3H_8 \cdot mol_{metal}^{-1} \cdot s^{-1}$ by the dispersion from EXAFS. Each measurement was conducted at four flowrates that were averaged with five injections each. The rates at each flow rate were then averaged to obtain the final catalytic rates that are included in this report. SMSI coverage was calculated using the ratio of the catalytic rate when re-reduced at 300-550 °C (SMSI) and re-reduced at 200 °C (non-SMSI).

## 2.5   CO infrared spectroscopy

CO infrared spectroscopy was performed on a Thermo Nicolet iS50 instrument with a mercury cadmium telluride (MCT) detector to determine the binding modes of the control and SMSI catalysts. Each spectrum was recorded by collecting 32 scans from 4000 to 650 cm$^{-1}$ at a resolution of 8 cm$^{-1}$. Spectra were collected until equilibrium had been achieved. This was done by scanning until there were no changes in spectra over time. The 0.1-1.0 wt% Ti containing catalysts were reduced in pure H$_2$ at 550 °C prior to analysis at 30 °C in pure CO. Ar was used to purge samples at 350 °C between gas treatments (pure Ar, 30 mL/min). Peaks were assigned for all catalysts as follows: atop bonding (2083 cm$^{-1}$), bridge bonding (1920-1950 cm$^{-1}$), and three-fold bonding (1840 cm$^{-1}$) which is consistent with past studies[30,33].

## 2.6   In situ X-ray absorption spectroscopy (XAS)

*In situ* XAS measurements were conducted at the 10-BM-B beamline at the Advanced Photon Source (APS) of Argonne National Lab at the Pd K edge (24.350 keV) to determine the Pd coordination environment and estimate particle sizes. The first set of measurements were conducting using catalysts that were pre-reduced from 250-550 °C. These catalysts were re-reduced at 200 °C for 30 minutes prior to scanning at room temperature in He. A second set of measurements were used to determine if particle sizes change after 350 °C oxidation and 200 °C re-reduction as well as how much Pd in the sample becomes oxidized after each stage of oxidation. The catalysts were scanned at room temperature after each of the following steps: reduced at 550 °C, oxidized at 30 °C, oxidized at 200/300/350 °C, and re-reduced at 200 °C. All scans were conducted at room temperature. For this set, the reduced catalyst scans were taken under flowing 5% H$_2$/He and the oxidized samples were scanned under flowing He. All samples were ground into a fine powder, pressed into a 6-shooter sample holder, and sealed in a sample cell with Kapton end caps. A gas purifier was connected to the He tank used for analysis to reduce the possibility of O$_2$ exposure upon cell cooling. Samples were analyzed with flowing He or flowing H$_2$. Measurements had a Pd foil and a third ion chamber that were used for energy calibrations. XAS data was fit using winXAS 3.1. Least-squares regression fits of the k$^2$-weighted Fourier transform data from 2.5 to 11.5 Å$^{-1}$ in k-space were used to obtain the extended x-ray absorption fine structure (EXAFS) coordination parameters. The first shell was used to fit all spectra. All samples were fit using experimental phases and amplitudes as well as theoretical scattering paths using FEFF. An

$S_o^2$ value of 0.79 at a fixed coordination number of 12 for the Pd foil was used for all samples. All samples were then analyzed using theoretical scattering paths at controlled values of $\sigma^2$ for direct comparison.

### 2.7 Scanning transmission electron microscopy (STEM)

Samples for scanning transmission electron microscopy (STEM) were prepared by drop-drying 3 μL of a 1 mg/mL supported catalyst suspension onto a Cu grid. High-angle annular dark-field scanning transmission electron microscopy (HAADF-STEM) were obtained on an FEI Talos F200X S/TEM with a 200 kV X-FEG field-emission source. 100 particles were imaged and the corresponding average particle size and particle size distribution were determined.

## 3. Results

### 3.1 Catalyst synthesis

The 2Pd/SiO$_2$ (0 wt% Ti) catalysts were prepared by addition of Pd to SiO$_2$. At a pH of 11, the SiO$_2$ surface hydroxyls are deprotonated using NH$_4$OH. Addition of metal cations such as Pd(NH$_3$)$_4^{+2}$ leads to a strong Coulombic attraction and uniform surface coverage[34]. Calcination at moderate temperature leads to the formation of small metallic nanoparticles[35]. 2Pd-XTi/SiO$_2$ where X is the Ti wt% were prepared by addition of Ti to SiO$_2$ followed by Pd. All catalysts had 2 wt% Pd. The Ti was added via incipient wetness impregnation (IWI) of titanium(IV) bis(ammonium lactate) dihydroxide. The SMSI precursors were dried and calcined at 300 °C to remove the organic ligands. Pd was then added to all catalysts using IWI of tetraamminepalladium(II) nitrate. The catalysts were calcined at 450/600/700 °C and reduced at 250 °C.

### 3.2 Pd nanoparticle size effects and evidence for SMSI

#### 3.2a Calcination temperature

The effect of calcination temperature on Pd nanoparticle size was determined for catalysts with 0-1.0 wt% Ti loading. For this study, small sizes of ~2-4 nm are desirable in order to determine differences in CO uptake, propylene hydrogenation rates, and the CO IR spectra[36,37].

Pd CO chemisorption uptakes at 30 °C were used to determine relative changes in particle size with increasing calcination temperature. Propylene hydrogenation rates were also tested as a

second method to support these results. The catalysts were tested after calcination at 450, 600, or 700 °C followed by reduction at 200 °C (Table 1). This low temperature reduction is necessary to avoid SMSI coverage which also reduces the CO uptake and propylene hydrogenation rate. All catalysts have similar CO uptakes and catalytic rates at a given calcination temperature indicating that $TiO_2$ had little effect on the Pd nanoparticle size. The CO uptakes were 0.32-0.39 with 450 °C calcination, 0.12-0.15 with 600 °C calcination, and 0.06-0.08 mol CO / mol Pd with 700 °C calcination. The propylene hydrogenation catalytic rates follow a similar trend where increasing calcination temperature resulted in a drop in catalytic rate from 4.5-5.7 with 450 °C calcination, 2.5-4.2 with 600 °C calcination, and 1.2-1.7 mol $C_3H_8*mol_{metal}^{-1}*s^{-1}$ with 700 °C calcination. Similar CO uptakes and rates for the Ti containing catalyst indicate that the Pd nanoparticle sizes increased similarly as calcination temperature was increased. Calcination at 450 °C gave the highest CO chemisorption and hydrogenation rates; therefore, this calcination temperature was used to synthesize the smallest Pd nanoparticle sizes in all catalysts.

**Table 1:** CO chemisorption and propylene hydrogenation results at 30 °C for catalysts calcined at different temperatures then reduced at 250 °C

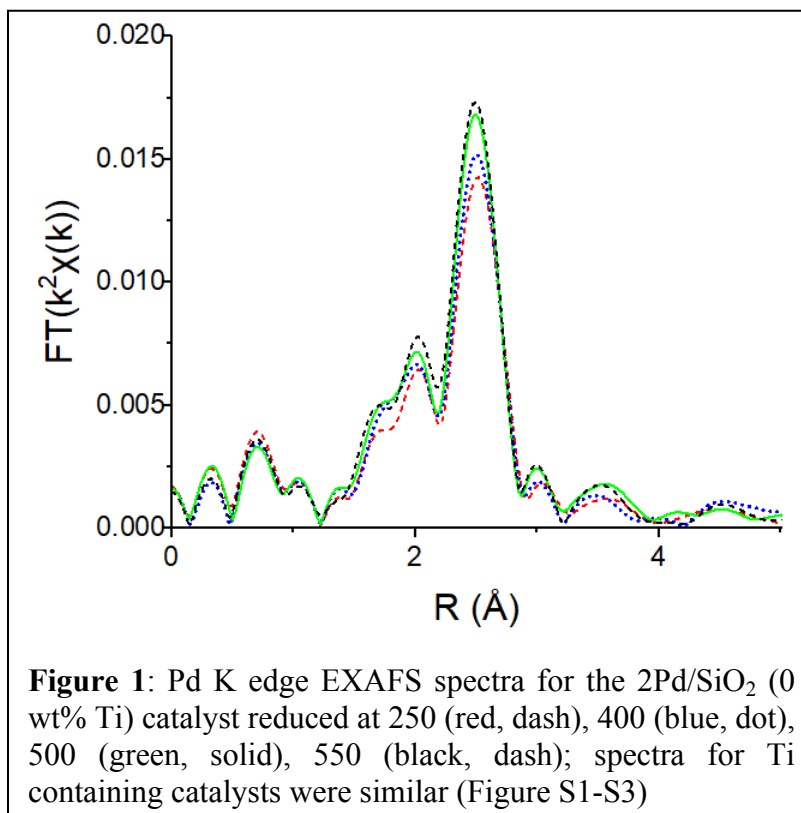| Calcination Temperature (°C) | Ti Loading (wt%) | CO Uptake (mol CO / mol Pd) | Catalytic Rate (mol $C_3H_8*mol_{metal}^{-1}*s^{-1}$) |
|---|---|---|---|
| 450 | 0 | 0.32 | 5.7 |
| | 0.1 | 0.39 | 5.1 |
| | 0.5 | 0.35 | 4.5 |
| | 1.0 | 0.33 | 4.6 |
| 600 | 0 | 0.15 | 3.5 |
| | 0.1 | 0.12 | 4.2 |
| | 0.5 | 0.15 | 3.8 |
| | 1.0 | 0.12 | 2.5 |
| 700 | 0 | 0.07 | 1.7 |
| | 0.1 | 0.08 | 1.3 |
| | 0.5 | 0.08 | 1.7 |
| | 1.0 | 0.06 | 1.2 |

*3.2b   Reduction temperature*

CO uptakes at 30 °C were calculated for the $2Pd/SiO_2$ (0 wt% Ti) catalyst calcined at 450 °C and reduced at 250-550 °C to determine how reduction temperature affects relative particle size. Increasing the reduction temperature decreased the CO uptake and the propylene hydrogenation

rate (Table 2). The rate decreased from 5.7 to 2.6 mol $C_3H_8$*$mol_{metal}^{-1}$*$s^{-1}$ and the CO uptake decreased from 0.32 to 0.12 mol CO / mol Pd when reduction temperature was increased from 250 to 550 °C. Since the CO:Pd ratio changes with Pd nanoparticle size, the particle size cannot be directly measured using chemisorption[38]. A more reliable method is needed that can also be used in the presence of SMSI. Thus, the effect of reduction temperature on particle size was tested using EXAFS of the Pd K edge to estimate Pd nanoparticle sizes from Pd-Pd first shell coordination[39].
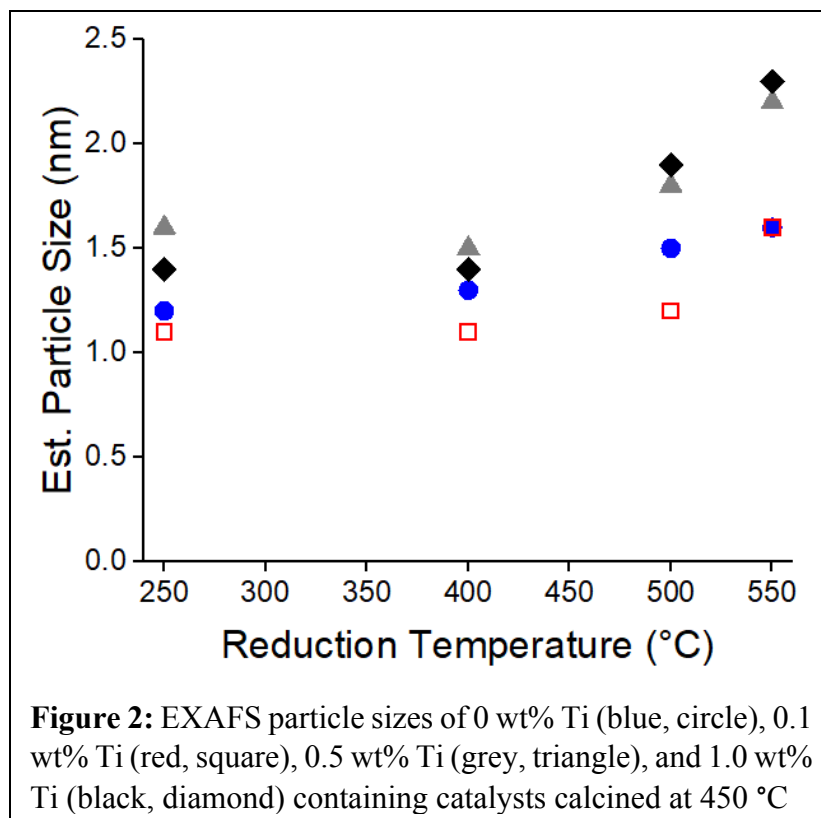
**Table 2:** CO chemisorption and propylene hydrogenation rate results at 30 °C for the 2Pd/SiO$_2$ (0 wt% Ti) catalyst calcined at 450 °C

| Ti Loading (wt%) | Reduction Temperature (°C) | CO Uptake (mol CO / mol Pd) | Catalytic Rate (mol $C_3H_8$*$mol_{metal}^{-1}$*$s^{-1}$) |
|---|---|---|---|
| 0 | 250 | 0.32 | 5.7 |
| | 400 | 0.25 | 5.5 |
| | 500 | 0.12 | 3.2 |
| | 550 | 0.12 | 2.6 |

In previous studies the Pt and Au NPs, M-M coordination number was shown to correlate with the nanoparticle size[39]. Thus, Pd K edge X-ray absorption fine structure (EXAFS) was used to determine the Pd-Pd coordination and the effect of increasing reduction temperature on particle size. Spectra were collected after reduction temperatures of 250/400/500/550 °C (Figure 1, Figure S1-S3). Coverage of the Pd nanoparticle surface by the



**Figure 1**: Pd K edge EXAFS spectra for the 2Pd/SiO$_2$ (0 wt% Ti) catalyst reduced at 250 (red, dash), 400 (blue, dot), 500 (green, solid), 550 (black, dash); spectra for Ti containing catalysts were similar (Figure S1-S3)

SMSI oxide will not affect the estimated particle sizes.

There are 3 main peaks between 1.5 and 3.0 Å in R space of the $k^2$-weighted magnitude of the Fourier transforms which is typical for scattering of Pd nanoparticles[40,41] (Figure 1). A Pd-Pd scattering path with a bulk bond distance of 2.75 Å was used to fit all samples. The phase and amplitude of the Pd foil (supported by theoretical scattering paths using FEFF) were used to



**Figure 2:** EXAFS particle sizes of 0 wt% Ti (blue, circle), 0.1 wt% Ti (red, square), 0.5 wt% Ti (grey, triangle), and 1.0 wt% Ti (black, diamond) containing catalysts calcined at 450 °C
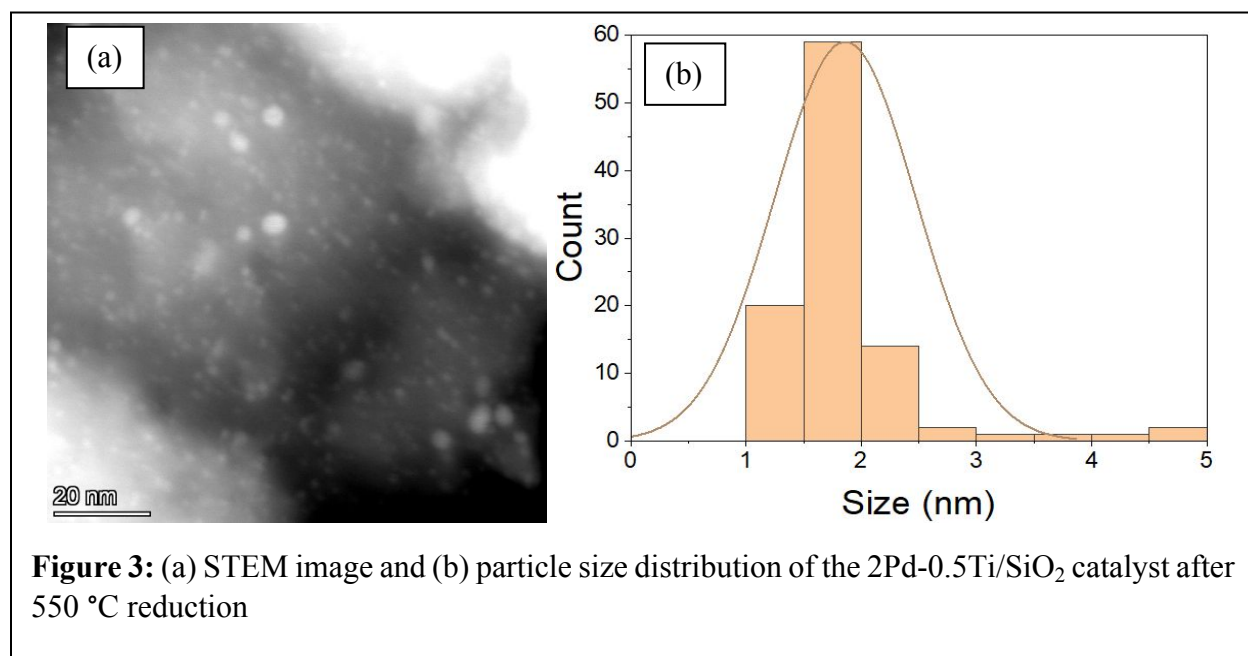
determine the EXAFS fitting parameters (Table S1). The bond distances were all 0.01-0.03 Å smaller than the bulk Pd bond distance of 2.75 Å. This is typical of small metal nanoparticles which experience bond contraction due to a high fraction of low coordination surface atoms[42]. The Pd nanoparticle size increased with increasing reduction temperature for all catalysts (Figure 2, Table S1). The particle sizes were 1.0-1.5 nm when reduced at 250 °C and grew to ~2 nm when reduced at 550 °C. When reduced at 700 °C, the sizes were all similar regardless of Ti loading and were about 4 nm. Since SMSI Pd surface coverage will be determined after reduction at 550 °C, all catalysts were pre-reduced at 550 °C in order that the size would not change after SMSI treatments.

To confirm the Pd nanoparticle size, STEM images were obtained on the catalysts after reduction at 550 °C. A typical STEM image and particle size distribution are shown for 2Pd-0.5Ti/SiO$_2$ (Figure 3). The average Pd nanoparticle size for each catalyst is given in Table 3 along with the sizes estimated by EXAFS. The STEM images and size distributions for the other catalysts are shown in Figure S4-S6.

**Table 3:** Particle sizes from EXAFS and STEM for catalysts reduced at 550 °C (EXAFS fittings included in Table S1 and STEM images and size distributions shown in Figure S4–S6)

| Ti Loading (wt%) | EXAFS Est. Size (nm) | STEM Size (nm) |
|---|---|---|
| 0 | 1.6 | $1.9 \pm 0.4$ |
| 0.1 | 1.6 | $1.9 \pm 0.8$ |
| 0.5 | 2.2 | $1.9 \pm 0.6$ |
| 1.0 | 2.3 | $1.9 \pm 0.4$ |



**Figure 3:** (a) STEM image and (b) particle size distribution of the 2Pd-0.5Ti/SiO$_2$ catalyst after 550 °C reduction
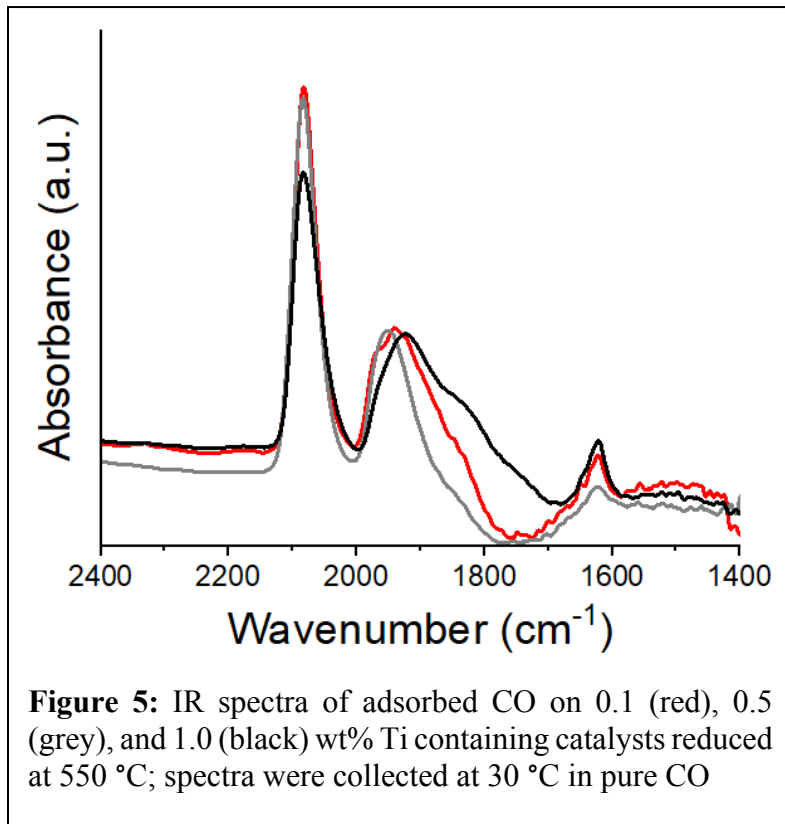
*3.2c Evidence for SMSI*

Propylene hydrogenation was used to show that an SMSI effect occurs for the low content Ti containing catalysts (Figure 4, Table S2). The Pd nanoparticle size was estimated from the Pd-Pd EXAFS coordination numbers. From the nanoparticle size, the fraction of surface Pd was



**Figure 4:** Apparent propylene hydrogenation TORs of all catalysts at 30 °C after 550 °C reduction
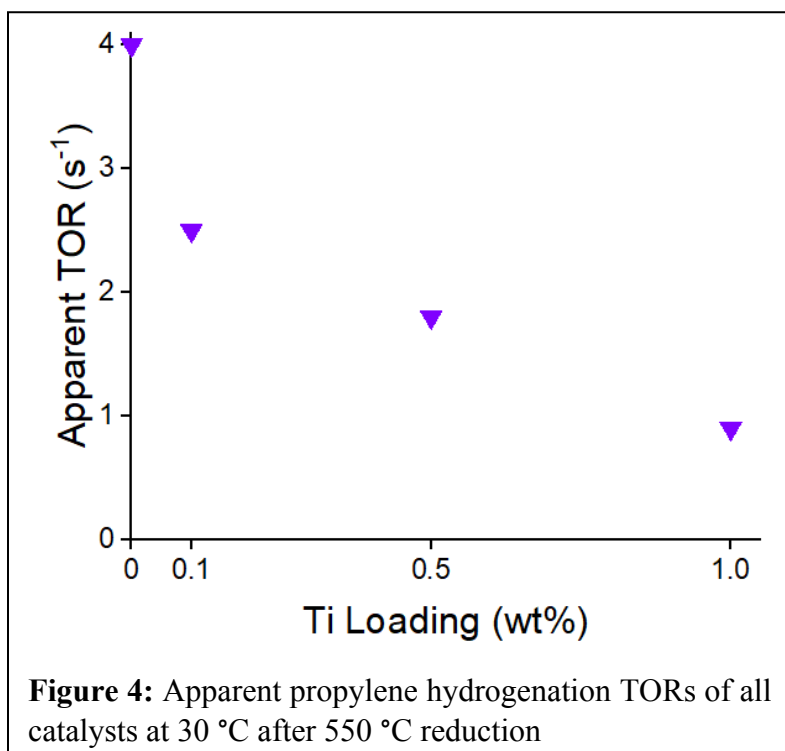
estimated. The fraction of Pd surface atoms was calculated as 1/Size (sizes used from Table 3). Since the catalysts were reduced at 550 °C prior to reaction, a portion of the surface Pd atoms were covered which lowers the catalytic rate. The propylene hydrogenation rates and fraction of surface Pd atoms were used to calculate the apparent TORs, i.e., assuming that there is no coverage and all Pd surface atoms are active. The apparent TOR decreases from 4.0 to 0.9 s$^{-1}$ as Ti loading is increased from 0 to 1.0 wt%. Propylene hydrogenation is a known structure-insensitive reaction; therefore, the TOR should be constant regardless of changes to particle size[43]. The lower TORs for the Ti containing catalysts are a result of Pd surface coverage by $TiO_{(2-x)}$ SMSI species, i.e., not all surface Pd sites are exposed. At 1.0 wt% Ti, for example, there is a loss of ~80% of the expected rate, indicating that ~80% of the Pd nanoparticle surface is covered by $TiO_{(2-x)}$. The results also indicate that lower Pd surface coverages can be obtained by lowering the Ti loading (Table S3). For example, at 0.1% Ti, the surface coverage is approximately 40%. Lower loadings may provide even lower surface coverages.

### 3.2e  Infrared spectra of adsorbed CO on SMSI Pd nanoparticles

The 0.1-1.0 wt% Ti containing catalysts calcined at 450 °C and reduced at 550 °C were analyzed using infrared (IR) spectroscopy of CO on Pd to determine which Pd surface sites are covered by the SMSI oxide. Face sites bond CO in a bridging or three-fold fashion while edge and corner sites bond CO linearly on a Pd nanoparticle[36]. The peaks at 2083 cm$^{-1}$ corresponds to atop CO bonding on Pd sites. The peaks at 1920-1950 cm$^{-1}$ and 1840 cm$^{-1}$ correspond to bridge and



**Figure 5:** IR spectra of adsorbed CO on 0.1 (red), 0.5 (grey), and 1.0 (black) wt% Ti containing catalysts reduced at 550 °C; spectra were collected at 30 °C in pure CO

three-fold bonding, respectively (Figure 5). The IR spectra of 2 nm Pd particles were previously reported and showed high ratios of bridge and threefold (higher order) to linear bonding CO[36,37]. After reduction at 550 °C, the IR spectra of the 2Pd-XTi/SiO$_2$ SMSI catalysts show a significant fraction of linear bonded CO and a strong reduction in bridge and threefold bonded CO compared to the 0Ti-2Pd/SiO$_2$ catalyst. The ratio of higher order (bridging and three-fold) to linear CO bonding indicates that even at 0.1 wt% Ti few threefold face sites bond CO while corner and edge sites remain exposed. The ratio of higher order to linear bonding peak areas was 0.8-1.2 for all three SMSI catalysts (Table 4) which is much lower than 2.8 for Pd nanoparticles of the same size.

**Table 4:** CO IR peak area ratios at 30 °C for catalysts reduced at 550 °C

| Ti Loading (wt%) | Higher Order to Linear Bonding Ratio |
|:---:|:---:|
| 0 | 2.8 |
| 0.1 | 1.2 |
| 0.5 | 0.8 |
| 1 | 1.0 |

*3.3   Reversibility of the SMSI state*

*3.3a   Removal of the SMSI overlayer*

Tauster, et al. showed that the adsorption capacity of metallic nanoparticles covered by SMSI oxides can be restored by oxidation at 500 °C followed by low temperature reduction at 175 °C[1]. For the 2Pd-XTi/SiO$_2$ catalysts, oxidation at 350 °C and re-reduction at 200 °C fully removed the SMSI coverage and final Pd nanoparticle sizes were the same as when initially reduced at 550 °C (Table 5) based on XAS (Table S4) and STEM analysis (Figure S7-S9).

14

**Table 5:** Particle sizes from EXAFS and STEM for catalysts reduced at 550 °C, oxidized at 350 °C, and re-reduced at 200 °C (EXAFS fittings included in Table S4 and STEM images and size distributions shown in Figure S7–S9)

| Ti Loading (wt%) | EXAFS Est. Size (nm) | STEM Size (nm) |
|---|---|---|
| 0 | 1.5 | - |
| 0.1 | 1.9 | $2.0 \pm 0.7$ |
| 0.5 | 2.3 | $1.8 \pm 0.6$ |
| 1.0 | 2.3 | $2.0 \pm 0.9$ |

The propylene hydrogenation TORs of the catalysts reduced at 550 °C, oxidized at 350 °C and re-reduced at 200 °C are show in Table 6. The catalytic rates were all similar and the average TOR was $5.5 \pm 1.3$ s$^{-1}$ was consistent with the literature for 1-3 nm Pd particles on alumina which had TORs of 4.4-12 s$^{-1}$ [44].

**Table 6:** Propylene hydrogenation results at 30 °C for catalysts reduced at 550 °C, oxidized at 350 °C, and re-reduced at 200 °C

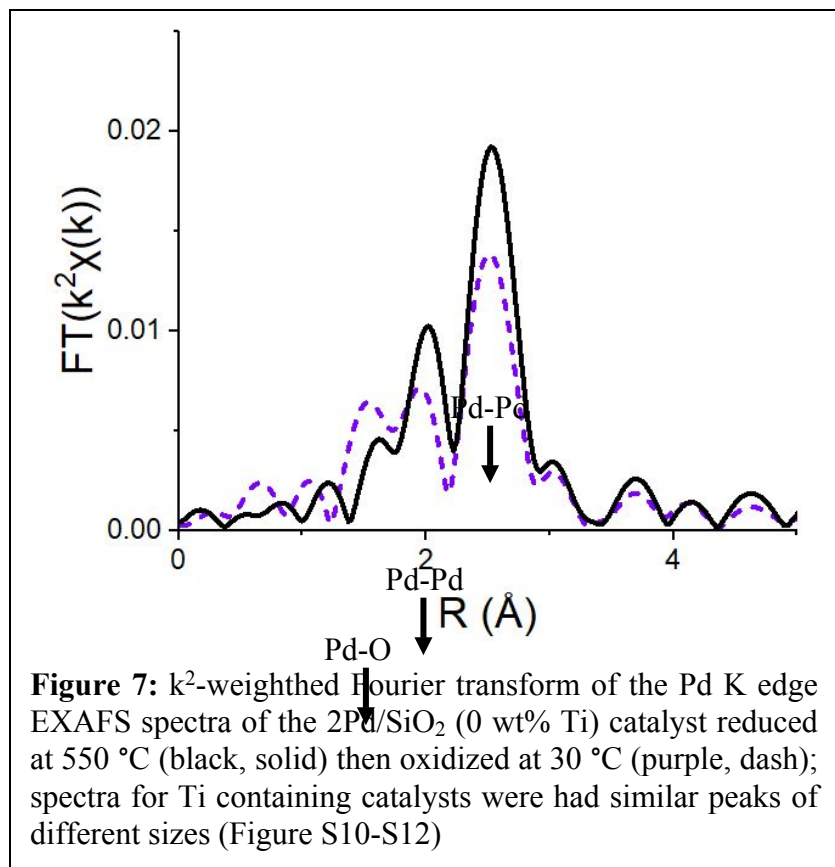| Ti Loading (wt%) | Rate (mol $C_3H_8$*mol$_{metal}^{-1}$*s$^{-1}$) | Dispersion | TOR (s$^{-1}$) |
|---|---|---|---|
| 0 | 2.6 | 0.64 | 4.0 |
| 0.1 | 2.7 | 0.57 | 4.7 |
| 0.5 | 3.1 | 0.44 | 7.0 |
| 1 | 2.7 | 0.44 | 6.1 |

Since the nanoparticle size does not change after 350 °C oxidation and low temperature reduction, the fractional surface Pd nanoparticle coverage can be determine by the ratio of the propylene hydrogenation rate after high temperature reduction (SMSI covered Pd nanoparticles) divided by the rate after oxidation and re-reduction where the SMSI oxide over layer has been fully



**Figure 6:** SMSI coverage for 0.1-1.0 wt% Ti catalysts reduced at 550 °C

removed (Table S3). Based on the rates with and without SMSI coverage, the fractional Pd nanoparticle surface coverage is shown to increase with increasing Ti loading (Figure 6).
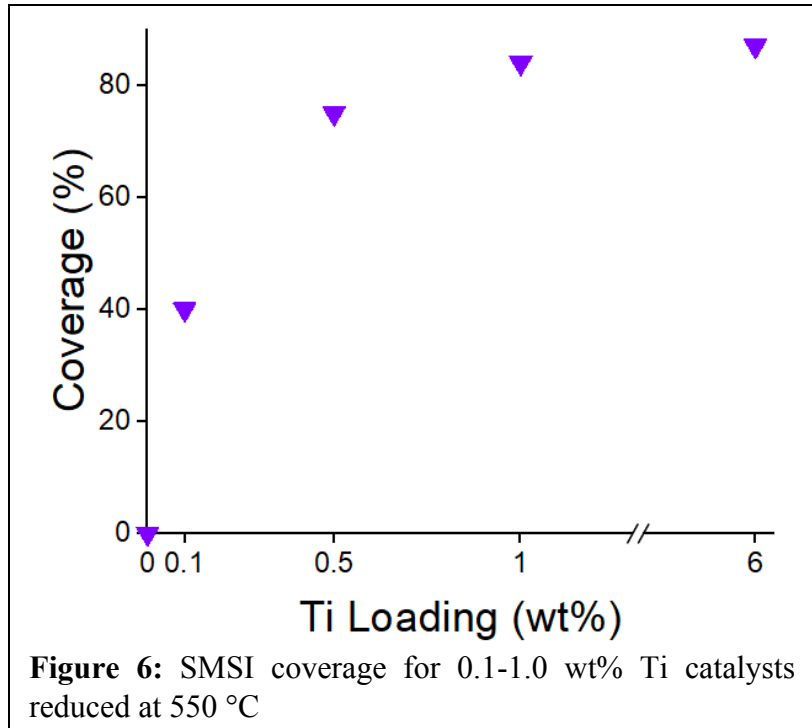
*3.3b    Oxidation at temperatures below 350 ℃*

While oxidation at 350 °C leads to a complete loss of the SMSI overlayer on the Pd nanoparticles, the catalysts were also oxidized at lower temperatures. All catalysts



**Figure 7:** $k^2$-weighthed Fourier transform of the Pd K edge EXAFS spectra of the 2Pd/SiO$_2$ (0 wt% Ti) catalyst reduced at 550 °C (black, solid) then oxidized at 30 °C (purple, dash); spectra for Ti containing catalysts were had similar peaks of different sizes (Figure S10-S12)
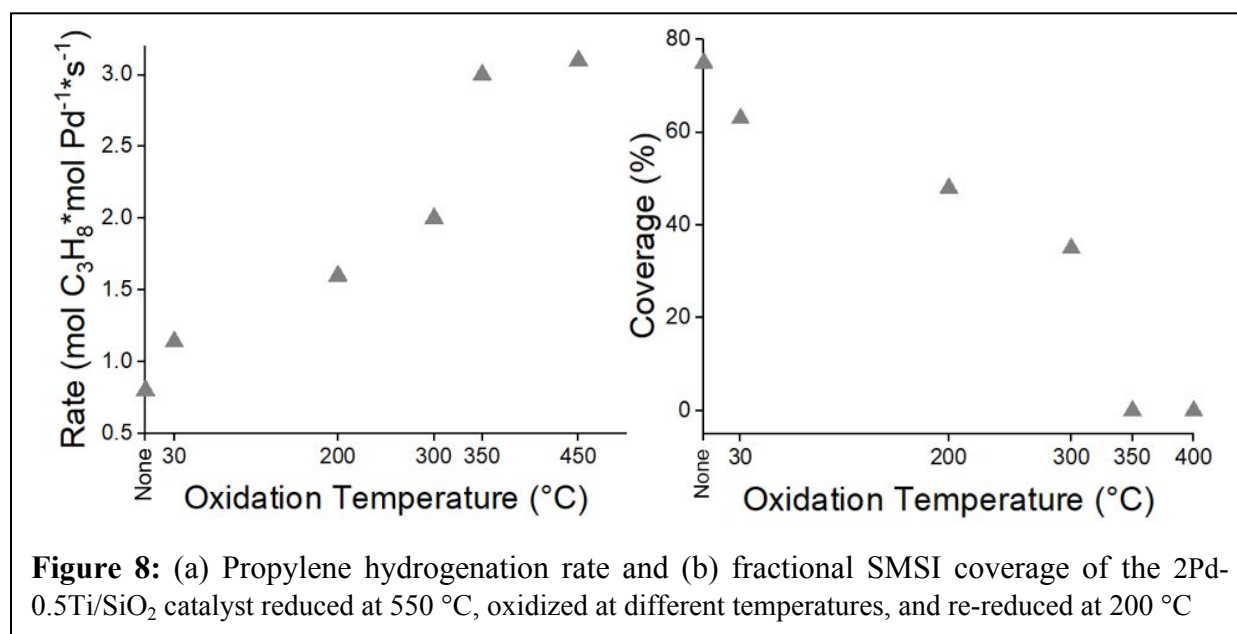
were analyzed using EXAFS to determine the fraction of Pd oxidized after 30 °C (Table 7). Partial

SMSI coverage will result in incomplete surface oxidation. At 30 °C only exposed surface Pd is

oxidized, and a new peak at 1.55 Å appears in the EXAFS due to PdO bond formation (Figure 7,

Figure S10-12). In addition, there is a loss of metallic Pd-Pd scattering peaks.

Based on the nanoparticle size determined from EXAFS and STEM (Table 3) and EXAFS

of the reduced Pd nanoparticles (Figure 1, Figure S1-S3), the fraction of surface Pd atoms in each

catalyst was estimated. The fraction Pd oxidized in each catalyst was determine from Pd-O

coordination numbers (CN) of the fits for 30 °C oxidized catalysts. For fully oxidized Pd there are

4 Pd-O bonds, thus the fraction of oxidized Pd in any catalyst is given by the Pd-O CN/4. The

surface fraction oxidized Pd decreases from 0.95 for 2Pd/SiO$_2$ to as low as 0.28 at 1.0 wt% Ti

(Table 7). This indicates that the SMSI overlayer prevents oxidation of the surface Pd atoms that

it covers. Increasing the Ti loading from 0.1 to 1.0 wt% increased the fraction of the nanoparticle

surface that was covered.

**Table 7:** Fraction of Pd nanoparticle surface covered by TiO$_{(2-x)}$ with increasing Ti loading;
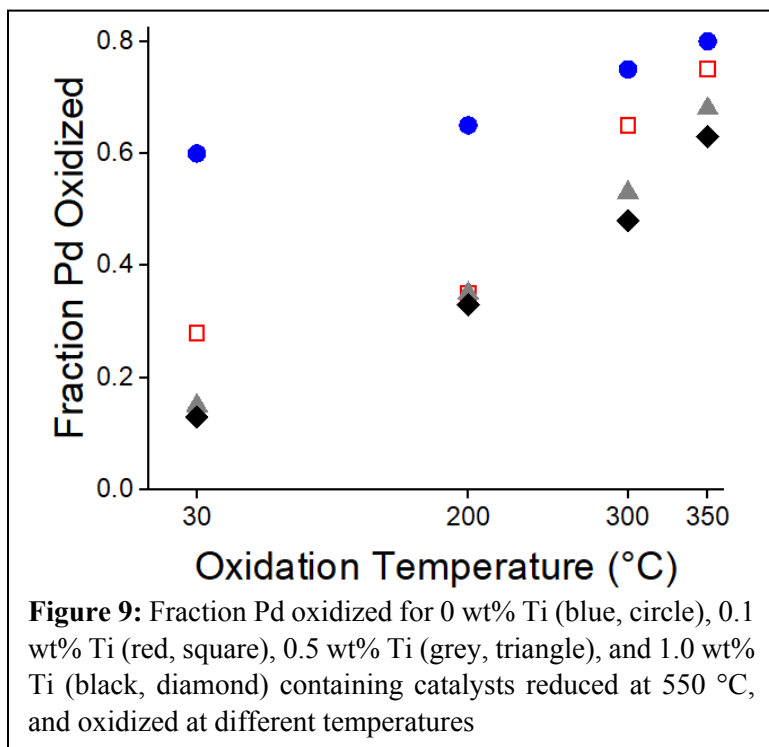catalysts were reduced at 550 °C and oxidized at 30 °C

| Ti Loading (wt%) | Surface Fraction Pd Oxidized | Fraction of Surface Pd Covered by SMSI |
|---|---|---|
| 0 | 0.95 | - |
| 0.1 | 0.44 | 0.54 |
| 0.5 | 0.33 | 0.66 |
| 1.0 | 0.28 | 0.72 |

The rate of propylene hydrogenation of SMSI covered Pd nanoparticles initially reduced at 550 °C was determined after oxidation with increasing temperature and re-reduction at 200 °C. For the 2Pd-0.5Ti/SiO$_2$ catalyst, the rate increases with increasing oxidation temperature suggesting that increasing oxidation temperatures partially removes the SMSI overlayer (Figure 8a, Table S5). Above 350 °C, the catalytic rate remained constant at ~3.1 mol C$_3$H$_8$*mol$_{metal}^{-1}$*s$^{-1}$ corresponding to a TOR of 6.8 s$^{-1}$ which is consistent with past studies of ~2 nm Pd particles[44] suggesting there is little to no SMSI coverage remaining.



**Figure 8:** (a) Propylene hydrogenation rate and (b) fractional SMSI coverage of the 2Pd-0.5Ti/SiO$_2$ catalyst reduced at 550 °C, oxidized at different temperatures, and re-reduced at 200 °C

The remaining coverage can be measured for the samples when oxidized below 350 °C, i.e., the rates after oxidation at low temperature and re-reduction at 200 °C divided by the rate after complete removal with 350 °C oxidation and 200 °C re-reduction (Figure 8b, Table S5). For 2Pd-0.5Ti/SiO$_2$, the Pd nanoparticle surface coverage is 75% after 550 °C reduction and no oxidation. Using an oxidation step with increasing temperature and re-reduction at 200 °C results in a lower SMSI coverage. Thus, the oxidation temperature can be used to control the SMSI coverage, at least for low temperature reactions.

The fraction of total Pd that was oxidized with increasing temperature was determined by EXAFS. As the oxidation temperature increased the Pd-O coordination number increased (Table S6). Since fully oxidized PdO has a coordination number of 4, the fraction of oxidized Pd with increasing temperature was estimated by determining the catalysts Pd-O CN/4. Increasing the oxidation temperature increases the fraction of oxidized Pd in all



**Figure 9:** Fraction Pd oxidized for 0 wt% Ti (blue, circle), 0.1 wt% Ti (red, square), 0.5 wt% Ti (grey, triangle), and 1.0 wt% Ti (black, diamond) containing catalysts reduced at 550 °C, and oxidized at different temperatures

catalysts (Figure 9). At 30° C exposed surface Pd atoms are oxidized. At higher oxidation temperatures Pd that is covered by the SMSI oxide is oxidized. At 350 °C, where there is little remaining SMSI coverage, there is also little metallic Pd. The EXAFS suggests that removal of the SMSI overlayer requires the oxidation of the metallic Pd covered by the SMSI oxide. For high coverages of the SMSI oxide this requires nearly complete oxidation of the metallic nanoparticle.


*3.4  Controlling partial SMSI coverage by increasing the re-reduction temperature*

As shown above, the fraction of SMSI coverage can be determined from the propylene hydrogenation rate at 30 °C with and without SMSI coverage. As demonstrated in Figure 6, the Pd nanoparticle coverage can be controlled by the Ti loading where coverages of less than ~50% would require ~0.2 wt% Ti or less. Additionally, the SMSI coverage for low temperature reactions can be controlled by oxidation of the SMSI catalyst at temperatures below 350 °C. While the SMSI overlayer can be removed at 350 °C, partial removal occurs at lower oxidation temperatures (Figure 8b).
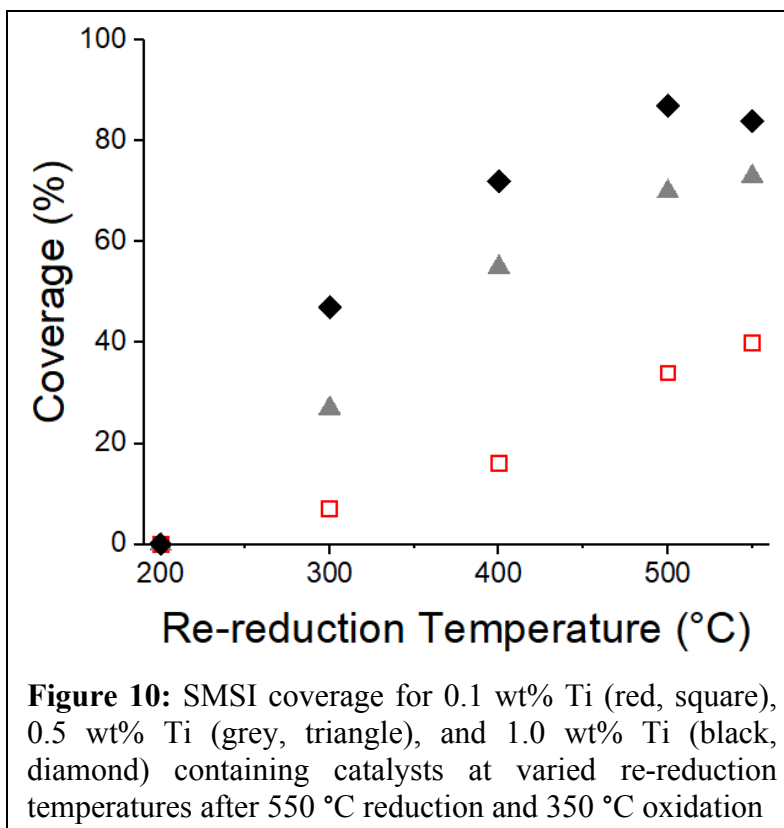
The 2Pd-XTi/SiO$_2$ (0.1–1.0 wt% Ti) SMSI catalysts were reduced at 550 °C, oxidized at 350 °C, and re-reduced at 200 °C through five oxidation and re-reduction cycles and the CO

chemisorption uptake was measured to confirm that there were no changes in particle size after these treatments. The initial and final CO chemisorption values were identical (Table 8) indicating no changes in nanoparticle size for oxidation and reduction temperatures below 350 °C and 550 °C, respectively.

**Table 8:** CO uptake for 2Pd-XTi/SiO$_2$ (0.1-1.0 wt% Ti) SMSI catalysts reduced at 550 °C, oxidized at 350 °C, and re-reduced at 200 °C after multiple oxidation and re-reduction cycles

| Ti Loading (wt%) | 200 °C Re-Reduction Measurement | CO Uptake (mol CO / mol Pd) |
|---|---|---|
| 0.1 | Initial | 0.29 |
| | Final | 0.28 |
| 0.5 | Initial | 0.26 |
| | Final | 0.28 |
| 1.0 | Initial | 0.21 |
| | Final | 0.22 |

The 2Pd-XTi/SiO$_2$ catalysts were reduced at 550 °C and oxidized at 350 °C to remove the SMSI overlayer. Each catalyst was subsequently re-reduced at increasing temperature from 200-550 °C. The propylene hydrogenation rate (measured at 30 °C) for each re-reduction temperature was divided by the rate of the catalyst re-reduced at 200 °C to determine the fraction of SMSI surface coverage (Figure 10, Table S7). For each Ti loading, the SMSI coverage increased with increasing reduction temperature. In addition, lower Ti loadings resulted in lower coverages at every reduction temperature. Decreasing the re-reduction



**Figure 10:** SMSI coverage for 0.1 wt% Ti (red, square), 0.5 wt% Ti (grey, triangle), and 1.0 wt% Ti (black, diamond) containing catalysts at varied re-reduction temperatures after 550 °C reduction and 350 °C oxidation
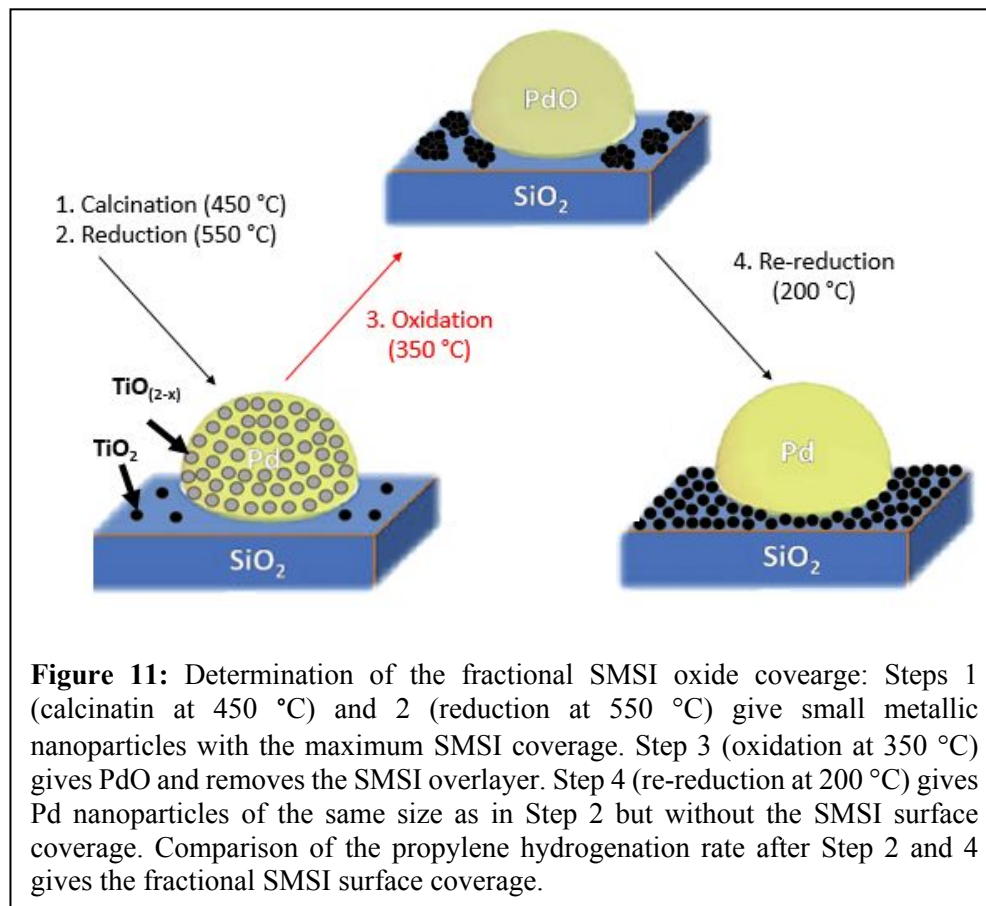
temperature resulted in lower levels of coverage from ~10% after 300 °C re-reduction to ~35% after 500 °C re-reduction for 0.1 wt% Ti. For 1 wt% Ti, 84% of the catalytic surface was covered after 550 °C reduction. Intermediate coverages of 0-75% were achieved with 200-400 °C re-reduction temperatures. These differences in coverage indicate that re-reduction temperature is also an effective method to vary particle coverage as long as the reaction temperature is below the re-reduction temperature.

## 4. Discussion

### *4.1 Evidence for SMSI and Conditions for Reversibility*

SMSI has been widely studied for metallic nanoparticles on oxide supports such as $TiO_2$[9], $CeO_2$[11,12], $Nb_2O_5$[15], $ZnO$[17,18], and on $SiO_2$ and supported SMSI oxides[2,4,15]. For the latter, the weight loadings of SMSI oxide are typically greater than 1.0 wt%. For both types, the NP surface is highly covered, often greater than 70%. In this study, we present three methods for controlling the SMSI coverage from 10-85%. To determine the Pd surface coverage by the SMSI oxide, one needs to compare the rate of propylene hydrogenation, a structure insensitive reaction in which the rate of every surface Pd is identical, with and without the SMSI overlayer. As shown by Tauster, et al. the SMSI oxide can be removed by oxidation at high temperature. For these 2Pd-XTi/$SiO_2$ catalysts, oxidation at temperatures of 350 °C led to nearly complete oxidation of the metallic Pd nanoparticles and reversal of the SMSI coverage. Re-reduction at 200 °C restored the Pd nanoparticles without formation of the SMSI overlayer. As shown by STEM and EXAFS, these treatments did not alter the Pd nanoparticle size. Comparison of the propylene hydrogenation rates for the SMSI and SMSI-free states allows for determination of the Pd surface coverage as shown in Figure 11.

**Figure 11:** Determination of the fractional SMSI oxide covearge: Steps 1 (calcinatin at 450 °C) and 2 (reduction at 550 °C) give small metallic nanoparticles with the maximum SMSI coverage. Step 3 (oxidation at 350 °C) gives PdO and removes the SMSI overlayer. Step 4 (re-reduction at 200 °C) gives Pd nanoparticles of the same size as in Step 2 but without the SMSI surface coverage. Comparison of the propylene hydrogenation rate after Step 2 and 4 gives the fractional SMSI surface coverage.

## 4.2  Partial coverage of Pd nanoparticles by $TiO_{(2-x)}$ SMSI oxides

The first method to control the Pd surface coverage is to control the Ti loading and reduce the catalyst at high temperature (550 °C) to give the maximum coverage for that loading. For example, with 0.1 wt% Ti, the Pd nanoparticle surface coverage is ~40%. While lower SMSI surface coverages were not investigated in this study, Ti loadings of less than 0.1 wt% would be expected to give even lower coverages. With 0.5 wt% Ti the surface coverage is ~75%. At coverages of 1% or higher, the Pd surface coverage is nearly constant at ~85% as seen in a previous study[2].

It is surprising that 0.1 wt% Ti can lead to a loss of 40% of the Pd surface sites. For example, on a 1.6 nm sized Pd nanoparticle in 2% Pd/SiO$_2$ the dispersion is 0.62. The ratio of surface Pd to Ti is approximately 6. In addition, not all of the $TiO_{(2-x)}$ would be expected to be near the Pd nanoparticles. In order for 0.1% Ti to reduce the catalytic rate by 40%, a high fraction of the $TiO_{(2-x)}$ would have to be covering the Pd nanoparticle surface and each $TiO_{(2-x)}$ species would

22

have to be covering more than one active site. Based on the IR spectra, the SMSI oxide selectively covers threefold Pd surface sites. Therefore, the SMSI oxide likely blocks more than one active site per Ti. If each SMSI oxide were to block three catalytic sites, this would require ~0.07% Ti to give a surface coverage of 40%. This also assumes that all of the Ti added to the catalyst is on the SMSI oxide with little remaining on the support. This suggests that at low loadings much of the $TiO_{(2-x)}$ is near or covering the Pd nanoparticles. High resolution electron microscopy techniques such as EDX may prove useful in determining this as well as the local structure of the partial SMSI overlayer.

The second method to control the Pd nanoparticle coverage by the SMSI oxide is to re-reduce the SMSI-free catalyst (Step 4 in Figure 10) at increasing temperatures. While there is little SMSI coverage upon reduction at 200 °C, the SMSI coverage increases at temperatures from 300-550 °C as seen in Figure 10. Re-reduction combined with low Ti loading gives surface coverages as low as 10%. The limitation of this method is that, to maintain the low surface coverage, the reaction temperature must be lower than the re-reduction temperature. However, by reducing the Ti loading, one can get the same surface coverage at a higher temperature. For example, with 0.1 wt% Ti a surface coverage of 30% is achieved using re-reduction at ~500 °C while for 0.5 wt% Ti the same surface coverage is possible using re-reduction at 300 °C (Figure 10).

The third method for controlling the SMSI coverage is by using low temperature oxidation of the SMSI catalyst (Figure 7). Room temperature air exposure of the SMSI covered Pd nanoparticle resulted in oxidation of the exposed metallic Pd atoms. Room temperature air is well known to oxidize metallic surface atoms in noble metal catalysts and is the basis for the oxidation-reduction chemisorption method. Re-reduction of the oxidized surface atoms does not lead to any significant changes in the fraction of metallic surface Pd, the fraction of SMSI coverage, or nanoparticle size. Thus, the SMSI oxide is impermeable to $O_2$ and the metallic Pd atoms under the SMSI oxide are not oxidized. Increasing the oxidation temperature, however, does oxidize a portion of the metallic Pd covered by $TiO_{(2-x)}$. Re-reduction at 200 °C gives nanoparticles of the same size but with a higher fraction of exposed Pd. The fraction of exposed metallic Pd increases with increasing oxidation temperature until 350 °C where the SMSI oxide no longer covers the metallic Pd nanoparticles and the surface is fully metallic after 200 °C re-reduction. Oxidation at 350 °C leads to nearly complete oxidation of the metallic Pd nanoparticles. Thus, to remove the SMSI overlayer, one needs to oxidize the metallic atoms at the Pd-SMSI oxide interface. Since the

SMSI oxide is impermeable to $O_2$ and the fraction of oxidized Pd increases with increasing temperature, it is likely that oxidation of the SMSI covered Pd occurs at the edge of the SMSI oxide. As the temperature increases, sub-surface Pd oxidizes until the SMSI surface covered Pd is oxidized and the SMSI-Pd interface is fully removed. Removal of the SMSI oxide requires oxidation of the covered Pd atoms rather than migration of the SMSI oxide away from the Pd nanoparticle resulting surface oxidation and complete removal of the overlayer.

### 4.3   Controlling partial coverage for improved SMSI catalysts

The presence of the SMSI oxide has been shown to be beneficial for several catalytic reactions[2-8]; however, the high surface coverage of active sites leads to low rates. SMSI catalysts most often improve selectivity by suppressing hydrogenolysis reactions. The desired reaction rate, however, is also greatly reduced. Thus, the SMSI catalyst has improved selectivity but at a low rate. The latter is fractional compared to the rate of the SMSI-free catalyst.

For example, dehydrogenation of propane on ~2 nm Pt nanoparticles supported on $SiO_2$ had a 60% propylene selectivity and 40% hydrogenolysis selectivity to methane and ethane at 30% conversion[2]. Addition of SMSI oxides, for example Pt-Ti/$SiO_2$ and Pt-Nb/$SiO_2$ catalysts with 3% Ti and 4% Nb, suppressed hydrogenolysis giving propylene selectivities above 95%. As observed for these catalysts, the SMSI oxides resulted in the loss of over 80% of the active sites.

Similarly, Yang, et al. prepared Ni-Mo/$SiO_2$ catalysts for m-cresol hydrodeoxygenation which is a biomass model compound[45]. Under reaction conditions the Ni is reduced to Ni nanoparticles which are known for their high hydrogenolysis selectivity. The Mo:Ni molar ratios were varied and the catalytic performance was determined. At low Mo:Ni ratios and at high reaction temperature there is a high selectivity for hydrogenolysis and formation of $CH_4$. At a Mo:Ni ratio near one hydrogenolysis is suppressed and hydrodeoxygenation leads to high selectivity to toluene. Further increases in the Mo:Ni ratio maintains the high selectivity but reduces the rates suggesting extensive coverage of active sites. Thus, controlling the active site coverage can lead to improved selectivity and higher rates.

The goal of this study was to determine if one can control the SMSI active site coverage to lower levels than is generally obtained with the hope of improving the rate while maintaining high selectivity. We demonstrate that the coverage can be controlled resulting in catalysts with higher activity; however, much lower SMSI loadings are required than what have typically been used.

The effect on selectivity will depend on the specific reaction; however, based on the IR spectra, it appears that the SMSI oxide at low coverages occupies threefold surface sites which are known to be active sites for hydrogenolysis, for example. This study provides another option for synthesis of catalysts with improved performance.

## 5. Conclusions

~2 nm sized 2 wt% $Pd/SiO_2$ catalysts with 0-1.0 wt% Ti were synthesized using calcination at 450 °C and reduction at 550 °C. Calcination and reduction at higher temperatures led to slightly larger nanoparticles. Catalysts containing 0.1-1.0 wt% $TiO_{(2-x)}$ had reduced CO chemisorption capacities and lower propylene hydrogenation rates compare to $Pd/SiO_2$ of the same size suggesting coverage of the Pd nanoparticles by the $TiO_{(2-x)}$ SMSI oxide. The Pd nanoparticle surface coverage increased with increasing Ti loading. Oxidation at 350 °C followed by reduction at 200 °C removed the SMSI overlayer and did not change the Pd nanoparticle size. Thus, the fractional coverage of the Pd nanoparticles was determined from the ratio of the propylene hydrogenation rate with SMSI coverage divided by that without SMSI coverage. For Ti loadings from 0.1 to 1.0 wt%, the SMSI coverage increased from about 40-85%. Surface coverage of 40% suggests that most of the Ti is covering the Pd nanoparticles and that each SMSI oxide species leads to the loss of more than one active site. Consistent with this conclusion, the IR spectra of adsorbed CO show that the SMSI oxides are selectively blocking Pd threefold sites.

Following oxidation at 350 °C, partial SMSI coverage can also be controlled by re-reducing at temperatures from 300-500 °C. The low temperature re-reduction can be combined with low Ti loadings to give surface coverages as low as 10%. To retain low surface coverage the reaction temperature must be lower than the re-reduction temperature; however, by reducing the Ti loading, one can get the same surface coverage at a higher temperature. Finally, the SMSI surface coverage can be controlled by oxidation at temperatures below 350 °C followed by re-reduction at 200 °C. With increasing oxidation temperature, EXAFS shows that there is an increasing fraction of oxidized Pd. At 350 °C, where the SMSI oxide is fully removed, the metallic Pd nanoparticles are nearly fully oxidized. These results suggest that oxidation of the metallic Pd is required to remove the SMSI oxide overlayer. By controlling the SMSI oxide loading to levels of less than 1 wt%, it is suggested that catalysts with high selectivity and improved activity are possible.

**Conflicts of interest**

There are no conflicts to declare.

**Acknowledgements**

**References**

[1]  Tauster, S. J.; Fung, S. C.; Garten, R. L., "Strong Metal-Support Interactions. Group 8 Noble Metals Supported on $TiO_2$", *J. Am. Chem. Soc.*, 1978, **100**, 170-175.

[2]  Zhu Chen, J.; Gao, J.; Probus, P. R.; Liu, W.; Wu, X.; Wegener, E. C.; Kropf, A. J.; Zemlyanov, D.; Zhang, G.; Yang, X.; Miller, J. T., "The effect of strong metal-support interaction (SMSI) on $Pt-Ti/SiO_2$ and $Pt-Nb/SiO_2$ catalysts for propane dehydrogenation", *Catal. Sci. Technol.*, 2020, **10**, 5973-5982.

[3]  Kim, W. J.; Kang, J. H.; Ahn, I. Y.; Moon, S. H., "Deactivation behavior of a $TiO_2$-added Pd catalyst in acetylene hydrogenation", *J. Catal.*, 2004, **226**, 226-229.

[4]  Kang, J. H.; Shin, E. W.; Kim, W. J.; Park, J. D.; Moon, S. H., "Selective hydrogenation of acetylene on $Pd/SiO_2$ catalysts promoted with Ti, Nb and Ce oxides", *Catal. Today*, 2000, **63**, 183-188.

[5]  Kang, J. H.; Shin, E. W.; Kim, W. J.; Park, J. D.; Moon, S. H., "Selective Hydrogenation of Acetylene on $TiO_2$-Added Pd Catalysts", *J. Catal.*, 2002, **208**, 310-320.

[6]  Jenness, G. R.; Schmidt, J. R., "Unraveling the Role of Metal-Support Interactions in Heterogeneous Catalysis: Oxygenate Selectivity on Fischer-Tropsch Synthesis", *ACS Catal.*, 2013, **3**, 2881-2890.

[7]  Rodriguez, J. A.; Liu, P.; Hrbek, J.; Evans, J.; Pérez, M., "Water Gas Shift Reaction on Cu and Au Nanoparticles Supported on $CeO_2(111)$ and $ZnO(000)$: Intrinsic Activity and Importance of Support Interactions", *Angew. Chem. Int. Ed.*, 2007, **46**, 1329-1332.

8   Kumar, A.; Ramani, V., "Strong Metal-Support Interactions Enhance the Activity and Durability of Platinum Supported on Tantalum-Modified Titanium Dioxide Electrocatalysts", *ACS Catal.*, 2014, **4**, 1516-1525.

9   Tauster, S. J.; Fung, S. C.; Baker, R. T. K.; Horsley, J. A., "Strong interactions in supported-metal catalysts", *Science*, 1981, **211**, 1121-1125.

10  Dulub, O.; Hebenstreit, W.; Diebold, U., "Imaging Cluster Surfaces with Atomic Resolution: The Strong Metal-Support Interaction State of Pt Supported on $TiO_2(110)$", *Phys. Rev. Lett.*, 2000, **84**, 3646-3649.

11  Datye, A. K.; Kalakkad, D. S.; Yao, M. H.; Smith, D. J., "Comparison of metal-support interactions in $Pt/TiO_2$ and $Pt/CeO_2$", *J. Catal.*, 1995, **155**, 149-153.

12  Campbell, C. T., "Electronic perturbations", *Nat. Chem.*, 2012, **4**, 597-598.

13  Willinger, M. C.; Zhang, W.; Bondarchuk, O.; Shaikhutdinov, S.; Freund, H. J.; Schlögl, R., "A Case of Strong Metal-Support Interactions: Combined Advanced Microscopy and Model Systems to Elucidate the Atomic Structure of Interfaces", *Angew. Chem. Int. Ed.*, 2014, **53**, 5998-6001.

14  Kast, P.; Friedrich, M.; Teschner, D.; Girgdies, F.; Lunkenbein, T.; d'Alnoncourt, R. N.; Behrens, M.; Schlögl, R., "CO oxidation as a test reaction for strong metal-support interaction in nanostructured $Pd/FeO_x$ powder catalysts", *Appl. Catal. A-Gen.*, 2015, **502**, 8-17.

15  Ahn, I. Y.; Kim, W. J.; Moon, S. H., "Performance of $La_2O_3$- or $Nb_2O_5$-added $Pd/SiO_2$ catalysts in acetylene hydrogenation", *Appl. Catal. A-Gen.*, 2006, **308**, 75-81.

16  Mo, S.; Zhang, Q.; Zhang, M.; Zhanq, Q.; Li, J.; Fu, M.; Wu, J.; Chen, P.; Ye, D., "Elucidating the special role of strong metal-support interactions in $Pt/MnO_2$ catalysts for total toluene oxidation", *Nanoscale Horiz.*, 2019, **4**, 1425-1433.

17  Liu, X.; Liu, M.H.; Luo, Y.C.; Mou, C.Y.; Lin, S.D.; Cheng, H.; Chen, J.M.; Lee, J.F.; Lin, T.S., "Strong Metal-Support Interactions between Gold Nanoparticles and ZnO Nanorods in CO Oxidation", *J. Am. Chem. Soc.*, 2012, **134**, 10251-10258.

18  Gao, J.; Sawant, K. J.; Miller, J. T.; Zeng, Z., Zemlyanov, D.; Greeley, J. P., "Structural and Chemical Transformations of Zinc Oxide Ultrathin Films on Pd(111) Surfaces.", *ACS Appl. Mater. Interfaces*, 2021, **13**, 35113-35123.

19  Tang, H.; Wei, J.; Liu, F.; Qiao, B.; Pan, X.; Li, L.; Liu, J.; Wang, J.; Zhang, T., "Strong Metal-Support Interactins between Gold Nanoparticles and Nonoxides", *J. Am. Chem. Soc.*, 2016, **138**, 56-59.

20  Liu, S.; Xu, W.; Niu, Y.; Zhang, B.; Zheng, L.; Liu, W.; Li, L.; Wang, J., "Ultrastable Au nanoparticles on titania through an encapsulation strategy under oxidative atmosphere", *Nat. Comm.*, 2019, **10**, 5790.

21  Dong, J.; Fu, Q.; Li, H.; Xiao, J.; Yang, B.; Zhang, B.; Bai, Y.; Song, T.; Zhang, R.; Gao, L.; Cai, J.;Zhang, H.; Liu, Z.; Bao, X., "Reaction-Induced Strong Metal-Support Interactions between Metals and Inert Boron Nitride Nanosheets", *J. Am. Chem. Soc.*, 2020, **142**, 17167-17174.

22  Farmer, J. A.; Campbell, C. T., "Ceria Maintains Smaller Metal Catalyst Particles by Strong Metal-Support Bonding", *Science*, 2010, **329**, 933-936.

23  Matsubu, J. C.; Zhang, S.; DeRita, L.; Marinkociv, N. S.; Chen, J. G.; Grahaw, G. W.; Pan, X.; Christopher, P., "Adsorbate-mediated strong metal-support interactions in oxide-supported Rh catalysts", *Nat. Chem.*, 2017, **9**, 120-127.

24  Lee, J.; Burt, S. P.; Carrero, C. A.; Alba-Rubio, A. C.; Ro, I.; O'Neil, B. J.; Jim, H. J.; Jackson, D. H.K.; Kuech, T. F.; Hermans, I.; Dumesic, J. A.; Huber, G. W., "Stabilizing cobalt catalysts for aqueous-phase reactions by strong metal-support interaction", *J. Catal.*, 2015, **330**, 19-27.

25  Alexeev, O. S.; Chin, S. Y.; Engelhard, M. H.; Ortiz-Soto, L.; Amiridis, M. D., "Effects of Reduction Temperature and Metal-Support Interactions on the Catalytic Activity of Pt/γ-$Al_2O_3$ and Pt/$TiO_2$ for the Oxidation of CO in the Presence and Absence of $H_2$", *J. Phys. Chem. B*, 2005, **109**, 23430-23443.

26  Han, B.; Guo, Y.; Huang, Y.; Xi, W.; Xu, J.; Luo, J.; Qi, H.; Ren, Y.; Liu, X.; Qiao, B.; Zhang, T., "Strong Metal-Support Interactions between Pt Single Atoms and $TiO_2$", *Angew. Chem. Int. Ed.*, 2020, **59**, 11824-11829.

27  Chu, M.; Pan, Q.; Bian, W.; Liu, Y.; Cao, M.; Zhang, C.; Lin, H.; Zhang, Q.; Xu, Y., "Strong metal-support interaction between palladium and gallium oxide within monodisperse nanoparticles: self-supported catalysts for propyne semi-hydrogenation", *J. Catal.*, 2021, **395**, 36-45.

28  Liu, X.; Liu, M.H.; Luo, Y.C.; Mou, C.Y.; Lin, S.D.; Cheng, H.; Chen, J.M.; Lee, J.F.; Lin, T.S., "Strong Metal-Support Interactions between Gold Nanoparticles and ZnO Nanorods in CO Oxidation", *J. Am. Chem. Soc.*, 2012, **134**, 10251-10258.

29  Zhang, S.; Plessow, P. N.; Willis, J. J.; Dai, S.; Xu, M.; Graham, G. W.; Cargneloo, M.; Abild-Pedersen, F.; Pan, X., "Dynamical Observation and Detailed Description of Catalysts under Strong Metal-Support Interaction", *Nano Lett.*, 2016, **16**, 4528-4534.

30  Polo-Garzon, F.; Blum, T.; Bao, Z.; Wang, K.; Fung, V.; Huang, Z.; Bickel, E. E.; Jiang, D.; Chi, M.; Wu, Z., "*In* Situ Strong Metal-Support Interaction (SMSI) Affects Catalytic Alcohol Conversion", *ACS Catal.*, 2021, **11**, 1938-1945.

31  Armbrüster, M., Schlögl, R.; Grin, Y., "Intermetallic compounds in heterogeneous catalysis - a quickly developing field", *Sci. Tecnhol. Adv. Mater.*, 2014, **15**, 034803.

32  Lee, J.; Burt, S. P.; Carrero, C. A.; Alba-Rubio, A. C.; Ro, I.; O'Neil, B. J.; Jim, H. J.; Jackson, D. H.K.; Kuech, T. F.; Hermans, I.; Dumesic, J. A.; Huber, G. W., "Stabilizing cobalt catalysts for aqueous-phase reactions by strong metal-support interaction", *J. Catal.*, 2015, **330**, 19-27.

33  Childers, D. J.; Schweitzer, N. M.; Shahari, S. M.; Rioux, R. M.; Miller, J. T.; Meyer, R. J., "Modifying structure-sensitive reactions by addition of Zn to Pd", *J. Catal.*, 2014, **318**, 75-84.

34  Regalbuto, J. R.; Schreier, M.; Hao, X. Spieker, W.A.; Kim, J.G.; Miller, J. T.; Kropf, J. A., "Toward a Molecular Understanding of Noble Metal Catalyst Impregnation," in *Studies in Surface Science and Catalysis, Preparation of Catalysts VIII*, 2002, **143**, 45-53.

35  Spieker, W. A.; Miller, J. T.; Kropf, A. J., Regalbuto, J.R., "An EXAFS study of the coordination chemistry of hydrogen hexachloroplatinate (IV) 2. Speciation of complexes adsorbed onto alumina", *Appl. Catal. A: Gen.*, 2003, **243**, 53-66.

36  Yang, C.; Wu, Z.; Zhang, G.; Sheng, H.; Tian, J.; Duan, Z.; Hyuntae, S.; Kropf, A. J.; Wu, T.; Krause, T; Miller, J. T., "Promotion of Pd nanoparticles by Fe and formation of a $Pd_3Fe$ intermetallic alloy for propane dehydrogenation", *Catal. Today*, 2018, **323**, 123-128.

37  Sheu, L. L.; Karpinski, Z.; Sachtler, W. M. H., "Effects of Palladium Size and Palladium Silicide Formation on Fourier Transform Infrared Spectra of CO Adsorbed on $Pd/SiO_2$ Catalysts", *J. Phys. Chem.*, 1989, **93**, 4890-4894.

[38] Tereshchenko, A.; Guda, A.; Polyakov, V.; Rusalev, Y.; Butova, V.; Soldatov, A., "Pd nanoparticle growth monitored by DRIFT spectroscopy of adsorbed CO", *Analyst*, 2020, **145**, 7534-7540.

[39] Miller, J. T.; Kropf, A.J.; Zha, Y.; Rebalbuto, J. R.; Delannoy, L.; Louis, C.; Bus, E.; van Bokhoen, J. A., "The effects of gold particle size on Au-Au bond length and reactivity toward oxygen in supported catalysts", *J. Catal.*, 2006, **240**, 222-234.

[40] Srabionyan, V. V.; Bugaev, A. L.; Pryadchenko, V. V.; Avakyan, L. A.; van Bokhoven, J. A.; Bugaev, L. A., "EXAFS study of size dependence of atomic structure in palladium nanoparticles", *J. Phys. Chem. Solids*, 2014, **75**, 470-476.

[41] Purdy, S. C.; Seemakurthi, R. R.; Mitchell, G. M.; Davidson, M.; Lauderback, B. A.; Deshpande, S.; Wu, Z.; Wegener, E. C.; Greeley, J.; Miller, J. T., "Structural trends in the dehydrogenation selectivity of palladium alloys", *Chem. Sci.*, 2020, **11**, 5066-5081.

[42] Szczerba, W.; Riesmeier, H.; Thünemann, A., "Bond length contraction in gold nanoparticles", *Anal. Bioanal.*, 2010, **398**, 1967-1972.

[43] Somorjai, G. A.; Carrazza, J., "Structure sensitivity of catalytic reactions", *Ind. Eng. Chem. Fundamen.*, 1986, **25**, 63-69.

[44] Lear, T.; Marshall, R.; Lopez-Sanchez, J. A.; Jackson, S. D.; Klaptöke, T. M.; Bäumer, M.; Rupprechter, G.; Freund, H.J.; Lennon, D., "The application of infrared spectroscopy to probe the surface morphology of alumina-supported palladium catalysts", *J. Chem. Phys.*, 2005, **123**, 174706.

[45] Yang, F.; LiBretto, N. J.; Komarneni, M. R.; Zhou, W.; Miller, J. T.; Zhu, X.; Resaco, D. E., "Enhancement of *m*-Cresol Hydrodeoxygenation Selectivity on Ni Catalysts by Surface Decoration of MoO$_x$ Species", *ACS Catal.*, 2019, **9**, 7791-7800.